A study of oxide traps and interface states of the silicon-silicon dioxide interface

A. R. Stivers and C. T. Sah
Department of Physics, University of Illinois, Urbana, Illinois 61801

(Received 17 September 1979; accepted for publication 15 August 1980)

Vacuum-ultraviolet light (10.2 eV) generated electrons or holes are injected into the oxide by dc biasing metal-oxide-semiconductor Al-SiO_2 capacitors with 2800-Å (1000 and 1100 °C) dry oxides annealed in dry oxygen at 600 or 800 °C. The injected charges are trapped in the oxide. The trapped charge density is determined by the capacitance-voltage method and its location by the photocurrent-voltage method. The trapped-hole charge injected under positive dc bias was found to be within 100 Å of the oxide-silicon interface. Trapping kinetic data revealed two donorlike neutral hole traps with hole capture cross sections of 6×10^{-14} and 1×10^{-15} cm^2. Both of these traps, after being positively charged by hole capture, were efficient electron traps with an electron-capture cross section of 3×10^{-13} cm^2. An acceptorlike electron trap with an electron-capture cross section of 1×10^{-15} cm^2 was also detected which anneals out during 800 °C anneal in dry oxygen. Little increase in the interface-state density was observed during the charge-injection and trapping experiments. Analyses of the annealing kinetics of these oxide traps suggest that the larger hole trap is an excess silicon center (trivalent silicon) and the smaller hole trap is an excess oxygen center (nonbridging oxygen).

PACS numbers: 73.40.Ns, 73.40.Sx

I. INTRODUCTION

The Si-SiO_2 interface, although very narrow,[1] is where most of the electrically active defects are found.[2] The interface region is sensitive to growth parameters,[3,4] radiation,[5] and stress.[6] These interface defect centers seriously affect the capacitance and conductance of the silicon surface space-charge layer and the underlying device characteristics.

Electrons or holes can be injected into SiO_2 from a silicon substrate by ultraviolet irradiation,[7] minority-carrier avalanche,[8] or by the heating of the carriers in the high electric fields that can exist in the channel of a metal-oxide-semiconductor field-effect transistor (MOSFET).[9] Electron-hole pairs are generated in SiO_2 by vacuum-ultraviolet (VUV) irradiation,[10] γ or x rays,[11] and energetic particles.[12] If the injected charge carriers are trapped in the oxide, then the properties of the semiconductor near the trapped charge will be altered.

This paper reports a study of trapping of electrons and holes generated near the surface of the SiO_2 by vacuum-ultraviolet (VUV) irradiation (10.2-eV photon) and the dependence of the trap densities on oxidation conditions at low oxidation temperatures.[13] An appropriate polarity dc voltage is applied to the gate so that either the VUV-generated electrons or holes will drift across the oxide to the Si-SiO_2 interface, where they are trapped. The densities and capture cross sections of the oxide traps are calculated from the dependence of trapped charge density on the injected charge. Thus, the densities of different species of oxide traps, as distinguished by their capture cross sections, can be measured. Conventional capacitance-vs-voltage measurements will reveal the net amount of charge at any given time. The photocurrent-voltage (4.88-eV photon) measurements are used to determine the location of the trapped charge. In Sec. II the device fabrication procedure is discussed. In Sec. III the various experimental methods are described. The measurements used are as follows: the VUV-bias injection method for injecting holes or electrons into the SiO_2; the capacitance-vs-voltage (C-V) method for measuring the oxide charge density; and the photocurrent-vs-voltage (photo I-V) method for measuring the oxide charge location. The oxide-charge-trapping kinetics are also discussed. The experimental results are presented in Sec. IV, and in Sec. V they are discussed in terms of an oxide defect annealing model. Conclusions are given in Sec. VI.

II. DEVICE FABRICATION

The top and cross-sectional views of the MOS capacitors used in this study are shown in Fig. 1. The device has a

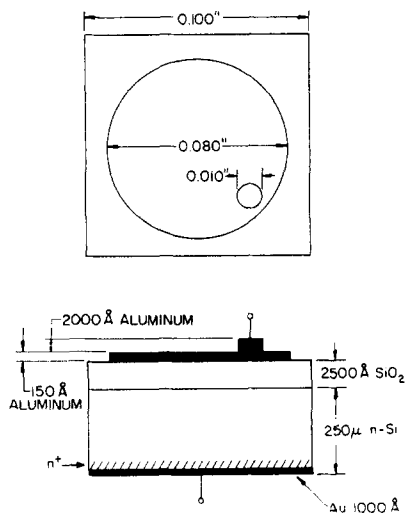

FIG. 1. Metal-oxide-semiconductor device structure used in this study.

 0021-8979/80/126292-13$01.10

large gate area (0.0324 cm^2) in order to have a high photocurrent. The gate metal (Al) is only 150 Å thick so as to be semitransparent to the ultraviolet radiation used in this study. The thick dot of Al on the gate is for wire bonding. A summary of the two series of MOS capacitors is given in Table I.

All devices used in this study were made on Si wafers from the same ingot. The silicon was Czochralski grown with a phosphorus donor density of 5×10^{14} cm^{-2}. The silicon slices were broken into convenient sizes in anticipation of splitting the device run by varying the oxidation conditions. After chemically thinning the slices down to 465 μm and standard cleaning, phosphorus from a P_2O_5 source was diffused into the Si slices at 1000 °C for 30 min. The phosphosilicate glass was etched off in dilute HF and the slices were then oxidized in dry O_2 at 1000 °C for 2 h. This resulted in 1000 Å of SiO_2 grown on the silicon which would seal the high-phosphorus-concentration n^+ layer. After the bottom surface of the Si slice was protected with wax, the oxide on the top surface was etched off in a dilute HF solution. The top surface was then chemically polished in a solution of HNO_3, HF, and CH_3COOH (6:1:1 by volume) until the Si thickness was 250 μm. This procedure completely removed the n^+ layer on the top surface.

The thermal oxides were then grown on the top surface. The "10" series in Table I was oxidized at 1000 °C for 9 h. The oxidation was followed by a 2-h anneal in dry argon at the oxidation temperature, giving 2750 Å of SiO_2. The "11" series was oxidized at 1100 °C for 3.25 h and annealed in Ar for 40 min, giving 2500 Å of SiO_2. All silicon pieces of each series were oxidized together. The wafers were slowly pulled out of the oxidation furnace with the furnace cap left on. When the temperature of the wafers reached 700 °C, they were pulled quickly to the mouth of the furnace tube. After the wafer temperature fell to 100 °C, the cap was removed and the wafers were taken out of the furnace.

Each of the series were split into five subseries. Four underwent a postoxidation heat treatment (POHT) in pure dry O_2 and the control series (10C and 11C) received no POHT. The POHT conditions were 600 °C for 1 or 10 h, and 800 °C for 1 or 10 h.

The gates were formed by first evaporating 150 Å of Al onto the oxide in an oil-diffusion-pumped vacuum system. The vacuum was then broken and the silicon pieces were placed on a metal mask. Then, 2000 Å of Al was evaporated through the mask to form the 10-mil-diam contact pads. The top surface was protected while the bottom surface oxide was etched off. Then 1000 Å of Au was evaporated onto the bottom surface, forming the Ohmic substrate contact. Standard photolithographic techniques were used to etch the 80-mil-diam gate. The pieces were then scribed and broken into chips. Each chip was then soldered at 90 °C to a transistor header using Plessey alloy 90 (20% Sn, 19% Pb, 13% Cd, 48% Bi) which melts at 76 °C. The gate lead was then ultrasonically bonded to the thick 10-mil-diam aluminum bonding pad.

TABLE I. Notation for device type as distinguished by oxidation temperature and postoxidation heat treatment. Example: 108T-2 is Device Type = 108T. Device No. = 2.

Post oxidation heat treatment	Oxidation temperature 1000 °C	1100 °C
No P. O. H. T. (Control)	10C	11C
600 °C for 1 h	1061	1161
600 °C for 10 h	106T	116T
800 °C for 1 h	1081	1181
800 °C for 10 h	108T	118T

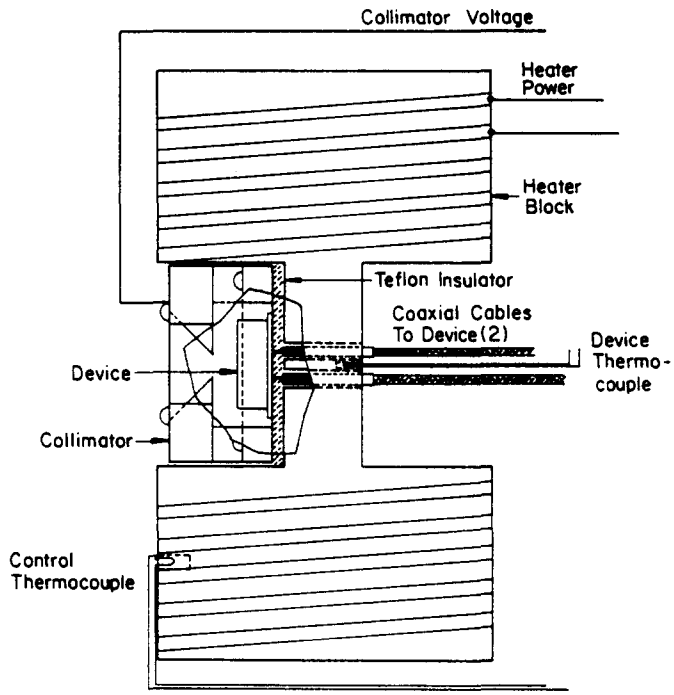

FIG. 2. Detail of the sample holder showing the placement of the device, collimator, and thermocouples.

III. EXPERIMENTAL METHODS

A. VUV-bias injection method

In order to study the trapping kinetics, electrons or holes were injected into the oxide. The VUV-bias method was chosen because it does not require high fields nor does the UV radiation penetrate the oxide. In this method, previously used by Powell and Derbenwick[10] and DiMaria, Weinberg, and Aitken,[14] vacuum-ultraviolet (VUV) light of 10.2-eV photon energy is shined on the device. 10.2 eV was chosen since: (i) it is the strong Lyman α line of hydrogen, (ii) it is greater than the SiO_2 band-gap energy, and (iii) it is near an absorption peak of SiO_2.[15] Electron-hole pairs are generated in the SiO_2 near the Al gate. By applying a positive voltage to the gate, holes may be drifted or injected into the oxide. By applying a negative voltage to the gate, electrons may be drifted or injected into the oxide.

The light source used was McPherson model 630 windowless discharge lamp. The Lyman α line was selected using a McPherson model 234 0.2-m monochromator. The sample was held in vacuum in a sample holder shown in Fig.

2. A collimator with a 0.085-in.-diam aperture is placed over the device to shield the header from the VUV radiation. Since the header is in electrical contact with the device substrate, photoelectron emission from the header would affect the substrate current measurement. To prevent photoelectrons emitted by the gate from reaching the header, a 300-V positive voltage was applied to the collimator. At this voltage, any change in the collimator voltage did not affect the substrate current. This was the criterion used to determine that there was no photoelectron component in the substrate current.

The substrate-current-measurement circuit is shown in Fig. 3 along with the capacitance-measurement circuit. The photocurrent is measured when the switch is connected to the I terminal. Currents of 50–40 nA were usually measured in the gate voltage range -20 to $+20$ V.

B. Oxide-charge measurement

Capacitance-vs-voltage curves were measured to determine the fixed oxide charge and interface states densities.[16] The capacitance and voltage data were taken in digital form by a computer automated-data-acquisition system. The capacitance data was taken with a $5\frac{1}{2}$-digit voltmeter and was averaged over 10 measurements. This was done to reduce the noise level to 0.02 pF, which is necessary in the strong accumulation region where the capacitance approaches the oxide capacitance asymptotically. The capacitance was measured at 1 MHz using a Boonton 72-A capacitance meter as shown in Fig. 3, with the switch set at position C.

The oxide charge and the interface state densities were evaluated as a function of the surface potential ψ_s using the method of Terman.[16] The value of the oxide charge at the flat-band condition, i.e., surface potential, $\psi_S = 0$, was used in the trapping kinetics analyses. The oxide capacitance was found by extrapolating the strong accumulation C-V data as done by McNutt and Sah.[17] The doping impurity density was calculated from low-temperature (130 K) depletion capacitance-vs-voltage characteristics. The theoretical capacitance-vs-voltage characteristic used in the Terman's analysis employed the analysis of Sah *et al.*[18] except in the case of inversion where the analysis of McNutt and Sah[19] was used.

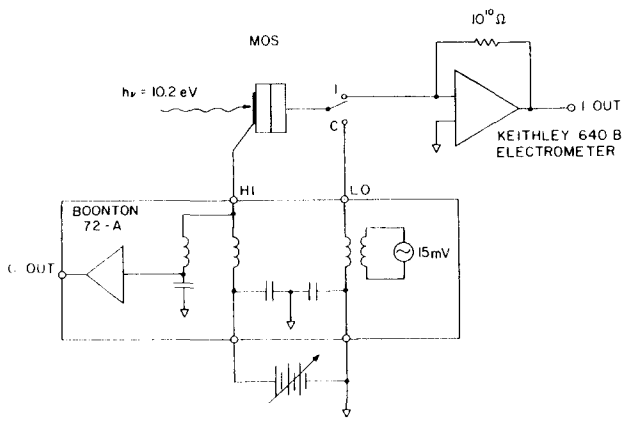

FIG. 3. Capacitance and photocurrent measurement circuits used during VUV-bias charge-injection experiments.

C. Oxide-charge location

Because the semiconductor capacitance depends on the electric field at the interface, the voltage shift of the capacitance-vs-voltage characteristic is due to that part of the oxide charge that induces an equal but opposite charge in the silicon. The C-V shift thus depends on the location of the oxide charge. In order to obtain the oxide-charge density, the charge centroid $\bar{x}$ must be known. The centroid is given by:

$$\bar{x} = \int_{-x_0}^{0} x\,\rho_0(x)\,dx \left[\int_{-x_0}^{0} \rho_0(x)\,dx\right]^{-1},$$

where $\rho_0(x)$ is the volume oxide charge density in C/cm^3 and x is the direction perpendicular to the interface with the Si-SiO_2 interface at $x = 0$ and the Al-SiO_2 interface at $x = -x_0 < 0$. Note that in this convention $\bar{x} \leqslant 0$.

The total areal oxide-charge density Q_0^T (C/cm^2) and the centroid can be separately determined by the photocurrent-vs-voltage method developed by DiMaria.[20] In this measurement, the MOS capacitor is exposed to ultraviolet light. Some of the light is absorbed by the gate and some more is absorbed by the silicon. The photoenergy is sufficient to excite the electrons at the aluminum Fermi surface or the silicon conduction band to energies above the SiO_2 conduction band edge. The electrons from the aluminum can be injected into the SiO_2 if a negative voltage is applied to the gate. The electrons from the silicon can be injected into the SiO_2 if a positive voltage is applied to the gate. The photocurrents measured by this method are known as internal photoemission currents.

Internal photoemission into a dielectric was studied by Berglund and Powell,[7] who found that the voltage dependence of the photocurrent arises from electron-phonon scattering in the image charge potential well. The image charge potential well narrows with increasing applied field. The photocurrent is thus a one-to-one function of the electric field at the injecting interface but outside the image charge potential well. The presence of charge in the oxide shifts the photo I-V characteristics along the voltage axis just as it shifts the C-V characteristics. The C-V shift should equal the silicon injecting photo I-V shift if the oxide charge is outside the image charge potential well. The aluminum-injecting photo I-V shift provides the extra information; it tells us how much oxide charge there is that induces an equal but opposite charge in the gate. The total oxide charge Q_0^T and the centroid $\bar{x}$ can be calculated from the silicon-injecting and aluminum-injecting photo I-V shifts, ΔV^+ and ΔV^- (Ref. 20)

$$Q_0^T = C_0(\Delta V^- - \Delta V^+), \tag{1}$$

$$\bar{x} = x_0 \frac{\Delta V^+}{\Delta V^- - \Delta V^+}, \tag{2}$$

where C_0 and x_0 are the oxide capacitance and oxide thickness, respectively. $\bar{x}$ is measured from the Si-SiO_2 interface and is negative.

Because at any practical field the image charge potential well has a finite width, the photo I-V method will not be sensitive to charge at the interface. A zero photo I-V shift together with a nonzero C-V shift indicates that there is

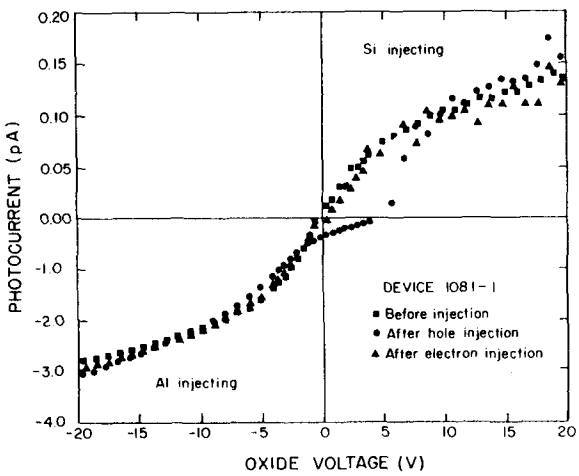

FIG. 4. Photocurrent-vs-voltage data of device 1081-1, typical of all photo *I-V* data taken.

charge very near the interface. The photo *I-V* data would put an upper limit of 50 Å to the distance that the charge can extend from the interface into the oxide.[14]

Figure 4 is a photo *I-V* data typical of all data taken. Note that the positive and negative photocurrents are plotted on different scales. The photocurrent injected from the silicon is smaller because the silicon is in the shadow of the semitransparent gate and thus gets less light. The device used here has an oxide grown at 1000 °C which subsequently received a 1-h heat treatment at 800 °C in dry O_2. The starting device (squares) has a flat-band voltage of -13.2 V. Also plotted is the data from the same device after injection of 6.6×10^{13} holes/cm^2 into the oxide (circles). 9.6×10^{11} holes/cm^2 were trapped during the injection, which caused the flat-band voltage to increase to -28.6 V. The third set of points (triangles) is from the same device after 4.3×10^{12} electrons/cm^2 were injected. The injected electrons neutralized most of the positive charge previously trapped, leaving a final flat-band voltage of -14.0 V. At the higher voltages, the data before and after hole injection are nearly coincident. There certainly is no -15-V flat-band-voltage shift in the silicon-injecting photo *I-V* characteristic as there is in the *C-V* curve. This is proof that there is no charge in the oxide bulk. 90% of the positive charge must be within 50 Å of the interface in this sample. The oxide charge that induces a *C-V* shift, $Q_0\equiv(1+\bar{x}/x_0)Q_0^T$, is therefore essentially equal to the total oxide charge Q_0^T, where $|x|<50$ A and $x_0=2800$ A.

Besides the positive charge near the Si-SiO_2 interface, in some devices *negative* charge near the Al-SiO_2 interface was found.

Between oxide voltages of -2 and 8 V there is an anomaly in the photo *I-V* data shown in Fig. 4. There is a large *negative* photocurrent at small positive oxide voltages. This effect was first reported and studied by DiMaria, Weinberg, and Aitken.[14] They found this effect to be due to injection from both interfaces. With a large positive charge trapped in the oxide, the photoexcited electrons in the aluminum, which normally would flow into the external gate lead under positive dc voltage applied to the aluminum, are attracted to the positive oxide charges. These aluminum electrons can be trapped in the oxide and possibly tunnel into silicon, creating an additional current opposite to the normal silicon → oxide → aluminum electron current. Because the aluminum received more light than the silicon, the extra photoelectron current injected from the aluminum into the oxide dominates. This effect was found to be most dramatic in devices that had an areally nonuniform oxide-charge distribution. Local high oxide fields due to nonuniformity exaggerate the Al → SiO_2 electron injection. The injection from both interfaces no longer happens after the electron injection neutralizes the positive charge, as shown by the triangles in Fig. 4.

The 4.88-eV photo *I-V* experiment works differently from the 10.2-eV VUV-bias injection experiment. The only similarity is that both used ultraviolet light to inject carriers into the oxide. The VUV-bias injection employs 10.2-eV vacuum ultraviolet light to create electron-hole pairs in SiO_2 at the Al-SiO_2 interface. Either the electron or the hole may be injected. The photocurrent densities used are high, as high as 1 μA/cm^2, in order that a significant amount of charge be injected and trapped. The photo *I-V* method used 5-eV light to inject only electrons into the oxide. 5-eV photons, unlike 10.2-eV photons, are transmitted through SiO_2. The current densities used during photo *I-V* measurements are kept low (~30 pA/cm^2) to minimize any change of the oxide-charge distribution due to trapping of the injected photoelectrons.

D. Determination of oxide-trap kinetic parameters

Charge injection has been used by various people to study both electron and hole traps in SiO_2.[21] The capture of the injected charge carriers can be described by the kinetic equation:

$$\frac{\partial p_T}{\partial t}=\sigma_p j_p p_T-\sigma_n j_n(N_{TT}-p_T), \tag{3}$$

where p_T is the density of captured holes at one species of oxide trap whose total density is N_{TT}. σ_p and σ_n are the hole and electron capture cross sections, respectively, and j_P and j_N are the hole and electron current densities, respectively. Here, thermal emission of trapped electrons and holes are neglected because the traps are deep (several electron-volt activation energy) within the SiO_2 band gap. j_N and j_p are assumed uniform throughout the oxide.

Integrating Eq. (3) yields:

$$p_T(t)=(N_{TT}-P_{T0})\{1-\exp[-\sigma_p N_{INJ}^{+}(t)]\}+P_{T0} \tag{4a}$$

for hole injection ($j_P\neq0$), and

$$p_T(t)=P_{T0}\exp[-\sigma_n N_{INJ}^{-}(t)]$$

for electron injection ($j_N\neq0$). P_{T0} is the trapped-hole density before injection. N_{INJ}^{+} and N_{INJ}^{-} are the areal densities of injected holes and electron, respectively. These are given by:

$$N_{INJ}^{+}(t)=\int_0^t |j_P(t')/q|\,dt', \tag{5a}$$

$$N_{\bar{INJ}}(t) = \int_0^t |j_N(t')/q|\, dt', \tag{5b}$$

N_{INJ} is the time integral of the conjuction currents j_P or j_N flowing into the gate. However, the experimental quantity measured is the substrate current j_S, which is given by

$$j_S = j_C - \frac{d}{dt} Q_S = j_P - \frac{d}{dt}(Q_{0X}^T + Q_{IS} + Q_S), \tag{6}$$

where j_C is the conduction current entering the substrate from the oxide, Q_{0X}^T is the total oxide-charge density, Q_S is the semiconductor space-charge density, and Q_{SS} is the interface state charge density. j_N replaces j_P in Eq. (6) for electron injection.

The gate voltage of an MOS capacitor can be related to the surface potential ψ_S, the work function difference

$\phi'_{MS}[\phi'_{MS} = \phi_M - (\chi_{Si} + |E_C - E_F|/q)]$,

the oxide capacitance C_0, and Q_{0X}^T, Q_S, and Q_{IS} by:

$$V_G = \phi'_{MS} + \psi_S - (1 + \bar{x}/x_0)Q_{0X}^T/C_0 - Q_S/C_0 - Q_{IS}/C_0. \tag{7}$$

Since the dc gate voltage is constant during the irradiation, the time derivative of Eq. (7) is as follows:

$$-\frac{d}{dt}(C_0\psi_S) = \frac{d}{dt}(Q_{0X}^T + Q_{IS} + Q_S) + \frac{\bar{x}}{x_0}\frac{d}{dt}(Q_{0t}^T). \tag{8}$$

Equations (5) can be rewritten in terms of measured quantities assumed $\bar{x} \approx 0$, as is found experimentally.

$$N_{INJ}^{+} = \int_0^t |j_S(t')/q|\, dt' - C_0\Delta\psi_S/q, \tag{9a}$$

$$N_{\bar{INJ}} = \int_0^t |j_S(t')/q|\, dt' - C_0\Delta\psi_S/q. \tag{9b}$$

It will be shown below that the oxide charge is very near the $Si\text{-}SiO_2$ interface. A change in the trapped-hole density in the oxide, p_T, will manifest itself as a change in the flat-band voltage of the C-V curve. By measuring the flat-band voltage during injection, one obtains data of $Q_{0X} + Q_{IS}$ versus N_{INJ}. Since there may be more than one trap species:

$$Q_{0X} = q\sum_i p_{Ti} + Q_1, \tag{10}$$

where Q_1 is independent of injection and p_{Ti} is the density of holes trapped at ith oxide trap species with density N_{TTi} and capture cross sections σ_{pi} and σ_{ni}. The measured values of $Q_{0X} + Q_{IS}$ are fitted to:

$$Q_{0X}(t) + Q_{IS} = q\sum_i N_{TTi}\{1 - \exp[-\sigma_{pi}N_{INJ}^{+}(t)]\} + \text{const} \tag{11}$$

for hole injection, where the initial hole concentration has been adjusted to zero in the experiment by electron injection. For electron injection one must fit:

$$Q_{0X}(t) + Q_{IS} = q\sum_i p_{T0i}\exp[-\sigma_{ni}N_{\bar{INJ}}(t)] + \text{const}. \tag{12}$$

The experiments were performed as follows: First, electrons are injected into the oxide by VUV light under negative gate bias to recombine with the trapped holes. A capacitance-voltage curve or flat-band voltage and the capacitance at the injection voltage are measured. Next, holes are injected into the oxide by VUV light and positive bias while the photocurrent is recorded on a strip-chart recorder. The photocurrent is integrated to give N_{INJ}^{+}. A C-V curve or flat-band voltage and the capacitance at the gate voltage during injection are again measured. The sequence of hole injection and capacitance measurements is repeated until saturation, i.e., negligible flat-band voltage change. ψ_S is calculated from the capacitance at the injection voltage. $\Delta\psi_S$ is the difference of two successive measurements. This yields a set of (Q_{0X}, N_{INJ}^{+}) data pairs to fit to Eq. (11). Then, electrons are injected by VUV light at a negative gate voltage while the photocurrent is measured to yield $N_{\bar{INJ}}$. After some electrons are injected, the C-V curve or flat-band voltage and the capacitance at the gate voltage during injection are measured to determine Q_{0X}. The electron-injection and capacitance measurements are repeated until the traps are discharged. This yields a set of $(Q_{0X}, N_{\bar{INJ}})$ data pairs to fit Eq. (12). Typically, 25–30 points are taken for each type of injection.

The present work used the trapping kinetics outlined above to discriminate between different species of oxide charge by measuring capture cross sections. The VUV-bias injection method is a powerful oxide-characterization tool. Many traps that are initially neutral can only be detected after they are charged. VUV-bias injection allows their detection and also provides a method to discriminate between traps.

IV. EXPERIMENTAL RESULTS

A. Interface state density

Figures 5–7 show the results of the interface state density measured at midgap, i.e., surface potential equal to the

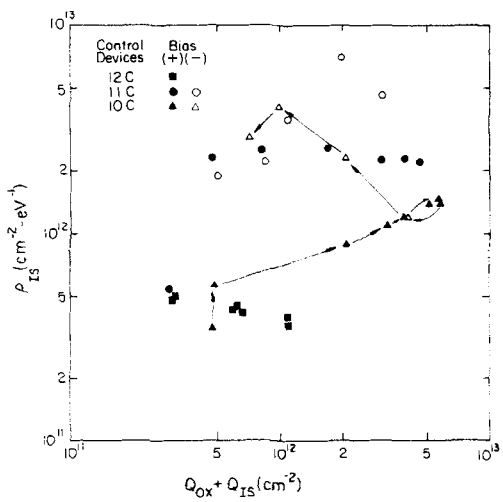

FIG. 5. Interface-state density vs total oxide charge for devices having undergone no postoxidation heat treatment. Both quantities are measured at midgap. The arrows show the time development of one device as holes were first injected (solid symbols), then electrons were injected (open symbols). The device types are explained in Table I.

bulk Fermi energy, versus total oxide charge at midgap. These data were taken during an oxide-charging experiment. Between irradiations of the samples with VUV light under positive gate voltage, C-V curves were taken and analyzed. Then the procedure was repeated with negative gate voltage. Each data point corresponds to one C-V curve. By plotting the interface state density ρ_{IS} versus $Q_{OX} + Q_{IS}$, one can show a dependence, if any, of ρ_{IS} on $Q_{OX} + Q_{IS}$.

Figure 5 shows the behavior of the control devices, 10 C, 11 C, and 12 C, which were oxidized at 1000, 1100, and 1200 °C. During hole injection ($V_G > 0$), $Q_{OX} + Q_{IS}$ increased monotonically. During electron injection ($V_G < 0$), $Q_{OX} + Q_{IS}$, decreased monotonically. The change in $Q_{OX} + Q_{IS}$, and ρ_{TTS} in time is indicated by the arrows. One must follow the solid figures from left to right then follow the open figures from right to left. The hole injection increases the $Q_{OX} + Q_{IS}$, of devices 10 C and 11 C by a factor of 10, while ρ_{IS} of device 10 C grows by a factor of 5 and the ρ_{IS} of device 11 C does not increase at all. There is a sharp rise in ρ_{IS} as electrons are injected, as shown by the sequences of open triangles and circles going from right to left. Since ρ_{IS} first increases then decrease during electron injection, we believe the increase to be an artifact due to nonuniform radiation of the gate producing a nonuniform oxide-charge distribution. Additional measurements of the interface state density using the low-temperature method confirm this finding. Thus, there is no strong dependence of ρ_{IS} on $Q_{OX} + Q_{IS}$.

Figure 6 shows similar data for devices oxidized at 1000 °C which underwent a postoxidation heat treatment. Here, again, $Q_{OX} + Q_{IS}$ of the devices varies by factors of 2–5 while ρ_{IS} barely changes. The large decrease in ρ_{IS} of device 1081 from the hole-injection ($V_G > 0$) to the electron-injection ($V_G < 0$) case is due to an improvement in the measured value of the doping density and not to a real generation of interface states. Figure 6 clearly shows no dependence of ρ_{IS} on $Q_{OX} + Q_{IS}$.

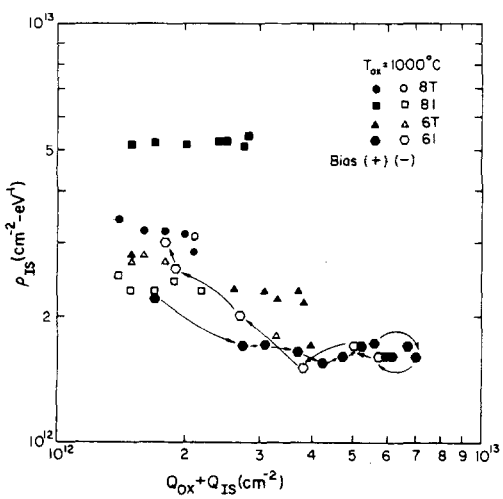

FIG. 6. Interface-state density vs total oxide charge for devices oxidized at 1000 °C. Both quantities were measured at midgap. The arrows show the time development of one device as holes first were injected (solid symbols), then electrons were injected (open symbols). The device types are explained in Table I.

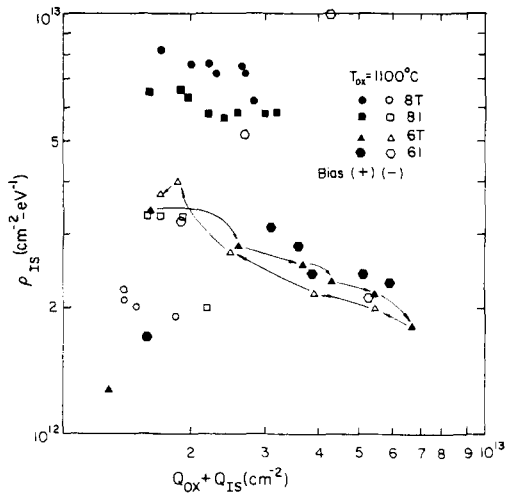

FIG. 7. Plot of the interface-state density vs total oxide charge for devices oxidized at 1100 °C. Both quantities were measured at midgap. The arrows show the time development of one device as holes first were injected (solid symbols), then electrons were injected (open symbols). The device types are explained in Table I.

Figure 7 contains the data for devices oxidized at 1100 °C. The conclusions are the same as that for the other devices. The interface state density is determined by the high-temperature processing steps and not by charging the oxide traps.

The high values of $Q_{OX} + Q_{IS}$, shown in Figs. 5–7 are due to the capture of photoinjected holes. Others[8,10,21] have found similar values after prolonged hole injection. Our devices have relatively thick (2800 Å) gate oxides, and it has been shown that a thick oxide gives higher oxide trap densities. The initial values of $Q_{OX} + Q_{IS}$ in our devices are larger than those in today's state-of-the-art devices. We have deliberately omitted certain processing steps that are known to reduce the oxide-charge density, such as heating in hydrogen at 400–550 °C, in order to preserve the oxide traps generated during oxidation.

The large values of $Q_{OX} + Q_{IS}$ are important for accurate data analysis. High-frequency capacitance measurements were used to measure the oxide-charge and interface-state densities because it is an efficient way to analyze the large amount of data taken. This method[16] is not accurate if $Q_{OX} + Q_{IS}$ is small.

The mobile-ion density in our sample was measured by stressing the oxide at $\pm$ 1 MV/cm for 10 min at 250 °C. The flat-band voltage shifts were typically 1 V or less. The mobile-ion density was therefore less than 10^{11} cm^{-2}, which is small compared with the oxide-charge and interface-state densities measured in these devices.

Various models have been proposed for interface states. One of us proposed that interface states are perturbed band states by the presence of trivalent silicon at the interface.[22] This model can explain the increase in oxide-trap density and the resultant increase in Q_{OX} and Q_{IS} after anneals in inert gas at elevated temperatures.[8] An inert-gas anneal should decrease the oxygen content in the oxide and therefore create more trivalent silicon and more interface states.

TABLE II. Results of fitting Q_{0X} and Q_{IS} to exponential functions during hole and electron injection in preliminary experiments.

	$Q_{0X}+Q_{IS}=-\Delta P_I \exp(-\sigma_p N_{INJ}^{+})+N_{TT}+\text{const}$ Hole injection			$Q_{0X}+Q_{IS}=\Delta P_I \exp(-\sigma_p N_{INJ})+\text{const}$ Electron injection		
Device	ΔP_I (10^{12} cm^{-2})	N_{TT} + const (10^{12} cm^{-2})	σ_p (10^{-13} cm^2)	ΔP_I (10^{12} cm^{-2})	Const (10^{12} cm^{-2})	σ_n (10^{-13} cm^2)
10C-2	6.02	6.34	1.22 ± 2%	4.1	0	4.5 ± 16%
1061-3	5.33	6.78	0.99 ± 3%	3.7	1.3	4.2 ± 13%
106T	2.48	3.53	1.55 ± 4%	1.72	1.13	7.0 ± 2%
1081-1	1.5	2.4	0.3 ± 17%	1.03	0.79	9.7 ± 2%
108T-2	0.89	1.84	0.96 ± 3%	1.01	1.02	8.8 ± 6%
11C-1	19	19	0.5 ± 14%	2.4	0.22	7.8 ± 2%
1161-1	17	18	0.6 ± 20%	3.32	1.3	7.5 ± 2%
116T-1	6.44	7.47	1.40 ± 2%	3.84	1.03	3.8 ± 8%
1181-2	1.88	2.88	1.4 ± 10%	1.19	1.07	9.5 ± 5%
118T-2	1.50	2.49	1.43 ± 5%			
Average			1.2			7.0

Charged trivalent silicon centers give a disorder to the interface potential. A strong potential well can split off a band state into the gap. Simple statistical arguments show that a random distribution of potential wells can cause tails of localized states to form, extending from the perfect crystal band edges into the gap.[23] The random interface potential is seen experimentally in interface conductance measurements[24] and near-threshold surface mobility measurements in field-effect-transistors.[25]

The initial interface-state density of the devices used in this study was high. This was a result of high-temperature processing steps designed to reduce the water annealing of the interface states. These states can be annealed by hydrogen, as discussed in Sec. IV B. Possibly the interface state density would have shown a dependence on the oxide trap if it was not so high before hole injection. The trapped holes in the oxide, which must be at many atomic bond distances from the interface, cannot cause as sharp an interface potential fluctuation as can charged defects at the interface. For this reason, the trapped holes may not have added enough additional disorder to the interface to generate more interface states.

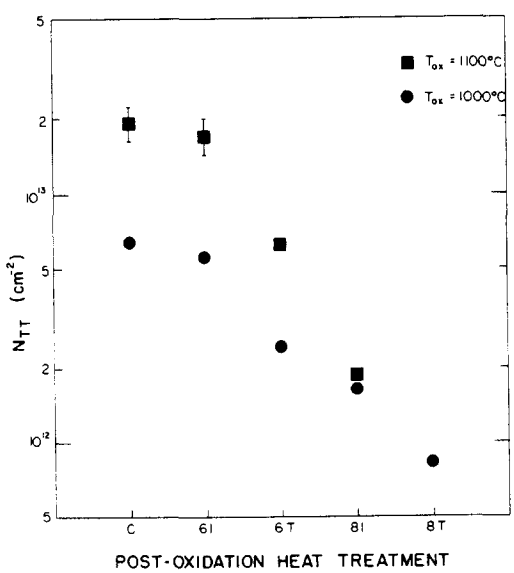

FIG. 8. Oxide trap density data from preliminary VUV-bias injection experiments (Table II) where the trapped-charge–vs–injected-charge data were fitted to only one exponential.

By varying the post oxidation anneal, the interface-state density can be varied independently of the sum of oxide and interface-state charge densities, $Q_{0X}+Q_{IS}$. By injecting holes or electrons into the oxide, $Q_{0X}+Q_{IS}$ can be varied without changing the interface-state density ρ_{IS}. Thus, the hole-trapping centers in the oxide that are detected here are different in structure or position from the defects that give interface states.

B. Oxide traps

The oxide traps in each device were characterized using the VUV-bias charge-injection technique. The initial data were taken when a windowed argon discharge with a trace hydrogen impurity was used as a VUV light source. This source was 500 times less intense than the windowless hydrogen discharge used later. Consequently, less charge was injected. Typically, $(2\text{–}4)\times10^{13}$ holes/cm^2 and 1×10^{13} electrons/cm^2 were injected. This level of injection allows detection of traps with hole-capture cross sections of 2×10^{-14} cm^2 or with electron-capture cross sections of 1×10^{-13} cm^2. The initial data could be fitted to a single exponential function, i.e., one term in Eqs. (11) and (12).

The results of the fits are given in Table II. The large spread of the capture cross sections is due to the insufficient number of points taken to allow accurate double exponential fits. More careful measurements, shown below, do not have as wide a range in fitted cross-section values. The average capture cross section of holes is 1.2×10^{-13} cm^2 and electrons is 7×10^{-13} cm^2.

In order to calculate the total oxide-trap density N_{TT}, one must subtract $Q_{0X}+Q_{IS}$ measured after infinite electron injection from $Q_{0X}+Q_{IS}$ measured after infinite hole injection. The columns labeled "N_{TT} + const" and "const" of Table II provide this information, "const" being the oxide charge in the absence of the trapped holes. N_{TT} + const − const is plotted in Fig. 8. The downward trend of N_{TT} from its initial value of the control device is clear. The abscis-

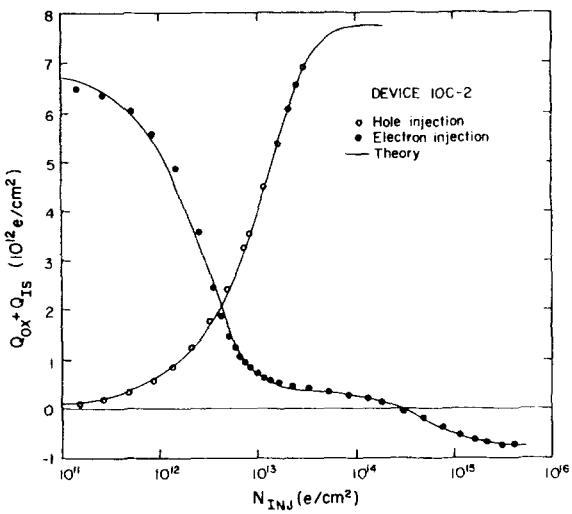

FIG. 9. Trapped charge vs injected charge of device 10C-2. One hole-capture cross section and two electron-capture cross sections are apparent.

sa is the severity (time and temperature) of the postoxidation heat treatment of each device type. The time dependence of the decrease will be discussed in Sec. V.

This method measures the total number of oxide traps, not just the trapped charge. The annealing of the number of traps with postoxidation heat treatment involves some structural changes and not just the neutralization of oxide charges. The results found in this study should not be confused with annealing results reported by others[5,10] which employed electron injection or irradiation with a negative voltage applied to the gate. Since our oxide traps are very close to the Si-SiO_2 interface, their thermal annealing must be related to the growth of the oxide at these relatively low temperatures.

During the 600 °C heat treatment in oxygen, the decrease in the number of traps is proportional to the number of oxide traps in the control device, i.e., before postoxidation heat treatment. This indicates that the annealing process is an ongoing destruction of the original traps and not a combination of trap generation and destruction. The constant of proportionality changes for the 800 °C heat treatment, but N_{TT} shows no indication of saturation.

The devices oxidized at 1000 °C (circular dots in Fig. 8) were selected for a more careful study of the trapping parameters. In this experiment a windowless hydrogen discharge was used as a light source. This lamp could induce photocurrents as high as 1 μA/cm^2 with 20 V across the device. Hole fluences as high as 2×10^{15} cm^{-2} and electron fluences as high as 6×10^{15} cm^{-2} were used. Such high fluences allow detection of hole-capture cross sections as low as 5×10^{-16} cm^2. Before the initial measurements, the devices were irradiated with VUV light at a negative gate voltage. The injected electron reduced the trapped-hole density to practically zero. The intention was to simplify the data interpretation by starting out with traps empty of holes or occupied by electrons.

The $Q_{OX}+Q_{IS}$-vs-N_{INJ} data was fitted to a single or double exponential. Holes were trapped easily in devices 10 C-2 and 1061-3 and could be accurately fitted to a single exponential or a single hole-capture cross section. Only 5×10^{13} holes/cm^2 could be safely injected in these devices. The flat-band voltage exceeded -90 V at this point and the injection had to be stopped to protect the device from oxide breakdown and to not exceed the limit of the instruments. This unfortunately limits the detection sensitivity of traps with small cross sections. The trends of the data from the other devices indicates that there are few small cross section traps in these two devices. The hole-injection data of devices 106T-2, 1081-2, and 108T-2 were fitted to two exponentials with capture cross sections that differed by a factor of 60. The electron-injected data of the three devices were also fitted to two exponentials.

The $Q_{OX}+Q_{IS}$-vs-N_{INJ} data for both electron and hole injections are shown in the next two figures. The data of device 10C-2 is plotted in Fig. 9. The theoretical curve fitted to the experiment is shown by the solid lines. The hole-injection data of device 10 C-2 (open circles) could be fitted to a single exponential. The electron-injection data (filled circles) were fitted to two exponentials, indicating two capture cross sections. At high injected-electron densities the net oxide and interface state charge, $Q_{OX}+Q_{IS}$, is negative. This is evidence of an electron trap. The data of device 106T-2 is plotted in Fig. 10. Here both the electron- and hole-injection data were fitted to two exponentials. Two hole-capture cross sections and two electron-capture cross sections are evident. $Q_{OX}+Q_{IS}$ before hole injection was significant, and this "built-in" positive charge prevented the electron trapping from making the final $Q_{OX}+Q_{IS}$ go negative.

The values of the fitting parameters are listed in Table III. The large hole trap has a hole-capture cross section of $\sigma_{p1}=6\times10^{-14}$ cm^2. The hole-capture cross section of the small trap, σ_{p2}, was less accurately measured but is about 1×10^{-15} cm^2. The densities of these two traps, N_{TT1} and N_{TT2}, are plotted in Fig. 11. The control device, 10 C-2, has the highest trap density of all devices shown here even though it had the least initial oxide charge. The large hole-trap density N_{TT1} decreases monotonically with increasing

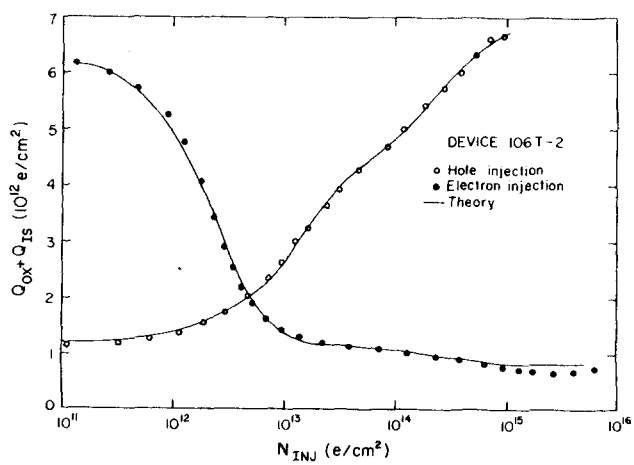

FIG. 10. Trapped charge vs injected charge of device 106T-2. Two hole-capture cross sections and two electron-capture cross sections are apparent.

TABLE III. Results of fitting charge-trapping data to Eqs. (11) and (12). Data were taken before anneal in forming gas.

Device	N_{TT1} (10^{12} cm^{-2})	σ_{p1} (10^{-14} cm^2)	N_{TT2} (10^{12} cm^{-2})	σ_{p2} (10^{-15} cm^2)	Q_p (10^{12} cm^{-2})
	Hole injection: $Q_{0X}+Q_{IS}=-N_{TT1}\exp(-\sigma_{p1}N_{INJ})-N_{TT2}\exp(-\sigma_{p2}N_{INJ})+Q_p$				
10C-2	7.70 ± 0.06	7.5 ± 0.1	...	...	7.72 ± 0.07
1061-3	6.44 ± 0.02	6.06 ± 0.04	...	...	7.89 ± 0.02
106T-2	2.87 ± 0.07	6.8 ± 0.3	2.71 ± 0.06	3.7 ± 0.3	6.74 ± 0.05
1081-1	1.55 ± 0.03	5.8 ± 0.3	3.41 ± 0.07	1.00 ± 0.05	6.02 ± 0.08
1081-2	1.38 ± 0.04	5.4 ± 0.4	3.21 ± 0.01	1.1 ± 0.1	5.6 ± 0.2
108T-1	1.18 ± 0.03	5.4 ± 0.4	2.9 ± 0.1	0.90 ± 0.08	5.1 ± 0.1
	Electron injection: $Q_{0X}+Q_{IS}=p_{T01}\exp(-\sigma_{n1}N_{INJ})+p_{T03}\exp(-\sigma_{n3}N_{INJ})+Q_n$				
Device	p_{T01} (10^{12} cm^{-2})	$\sigma_{n1}\leqslant\sigma_{n2}$ (10^{-13} cm^2)	p_{T03} (10^{12} cm^{-2})	σ_{n3} (10^{-15} cm^2)	Q_n (10^{12} cm^{-2})
10C-2	6.50 ± 0.09	3.2 ± 0.1	1.1 ± 0.1	1.6 ± 0.4	-0.71 ± 0.09
1061-3	6.2 ± 0.1	3.3 ± 0.4	0.5 ± 0.2	1 ± 1	0.9 ± 0.2
106T-2	5.29 ± 0.09	3.6 ± 0.2	0.4 ± 0.2	4 ± 5	0.8 ± 0.2
1081-1	3.76 ± 0.05	4.3 ± 0.1	...	...	1.38 ± 0.02
1081-2	3.23 ± 0.04	4.7 ± 0.2	...	...	1.31 ± 0.03
108T-1	3.29 ± 0.05	4.4 ± 0.2	...	...	1.03 ± 0.03

postoxidation heat-treatment severity. Figure 11 also shows the growth of the smaller hole-trap density N_{TT2}. The growth of N_{TT2} is always less than the decrease of N_{TT1}. The smaller hole trap was not detected in the device annealed for 1 h at 600 °C and no data for N_{TT2} at this condition are shown in Fig. 11 because of the low hole injection in this device. However, the apparent trend in Fig. 11 suggests that $N_{TT2}\approx1\times10^{12}$ cm^{-2}. The existence of such a density of the small trap would increase the trapped charge by only 4×10^{10} cm^{-2} when 4×10^{13} holes/cm^2 are injected into the oxide. This increase would be difficult to detect. The behavior of N_{TT1} and N_{TT2} in Fig. 11 shows that trap 1 was converted into trap 2 during the heat treatment. This will be used in a kinetic model to be discussed in Sec. V.

The electron-capture data is listed in Table III. Data from devices 10 C-2, 1061-3, and 106T-2 were fitted to two exponentials, while the rest were best fit to one exponential. Device 10 C-2 actually became negatively charged, so it appears that the second cross section is due to an acceptorlike electron trap. The 800 °C postoxidation heat treatments annealed out this trap completely while the 600 °C heat treatment annealed it partially.

The large electron-capture cross section σ_{n1} must be due to both of the hole traps, σ_{p1} and σ_{p2}. In order to compare the number of hole traps with the number of electron traps, one must take into account the occupation of the electron traps just before electron injection. Unlike the hole-injection case where the traps are empty of holes before irradiation, it is difficult to prepare the sample so that the traps are fully occupied with holes. Thus, the heights of the exponentials correspond to the initial trapped-hole densities and not the trap densities. In addition, there is a small decrease in trapped-hole density during the few minutes between the time when the hole injection ends and the electron injection begins. The decrease is due to either holes tunneling to the silicon or silicon electrons tunneling to the oxide traps. The high field at the charged interface promotes the tunneling process. The density immediately preceeding electron injection is $P_{P01}+P_{T03}+Q_n$. The sum of traps unoccupied by holes n_{Ti} at the beginning of hole injection is given by

$$\sum_i n_{Ti}=Q_p-p_{T03}-Q_n. \tag{13}$$

Table IV compares $N_{TT1}+N_{TT2}$ of the hole-capture data with $P_{T01}+\Sigma n_{Ti}$, indicating $N_{TT1}+N_{TT2}\gtrsim P_{T01}+N_{Ti}$. From this data it can be concluded that the electron-capture cross sections for the traps N_{TT1} and N_{TT2}, σ_{n1}, and σ_{n2} were too close to be resolved. Since $\sigma_{n1}\leqslant\sigma_{n2}$

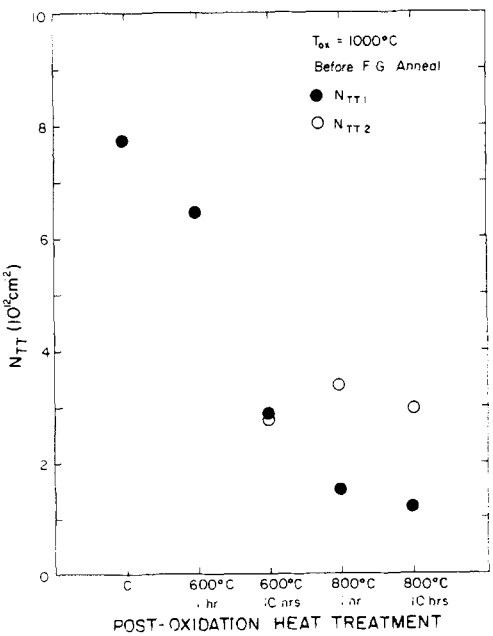

FIG. 11. Oxide trap densities for devices oxidized at 1000 °C and receiving various postoxidation heat treatments. N_{TT1} is the density of the trap with $\sigma_{p1}=6\times10^{-14}$ cm^2. N_{TT2} is the density of the trap with $\sigma_{p2}=1\times10^{-15}$ cm^2.

$= (3\text{–}6)\times 10^{-13}$ cm^2 is the size of a Coulombic attractive trap,[26] it is quite possible that the Coulomb force of these two traps is the determining factor of the electron-capture cross section rather than the detailed atomic makeup. σ_{n1} increases with hole trapping due to increasing N_{TT2} dominance. Thus, electron-capture cross section of hole trap 2 must be the larger of the two, $\sigma_{n2} \geqslant \sigma_{n1}$.

Four of the devices characterized above were annealed for 2 min at 400 °C in a forming gas (4% H_2, 96% N_2) ambient. The low-temperature method was used to determine the areal density of interface states before and after the anneal. The results are listed in Table V. A significant amount, 25–74%, did not anneal out. The hole-capture results are listed in Table VI. N_{TT1} was nearly the same as before the forming gas anneal (Table III). N_{TT2} decreased only for device 1081-2 from 3.21×10^{12} (Table III) to 1.24×10^{12} cm^{-2} (Table VI). The independence of N_{TT1} on a forming-gas anneal suggests that the OH^- or H^+ ion that annealed the interface states did not bond to the large oxide hole traps. Possibly this bonding did not take place because these traps were neutral before the anneal.

Table VI lists the electron-capture data for the devices after anneal in forming gas. The anneal eliminated the acceptorlike electron traps (σ_{n3} in Table III) but had little effect on the electron-capture cross sections σ_{n1} and σ_{n2} ($\sigma_{n2} \simeq \sigma_{n1}$).

In summary, the data showed two donorlike hole traps with hole-capture cross sections of $(6 \pm 1)\times 10^{-14}$ and $(5 \pm 2)\times 10^{-15}$ cm^2. The electron-capture cross sections of these traps after capturing a hole and becoming positively charged are both $(4 \pm 1)\times 10^{-13}$ cm^2. The two electron-capture cross sections were too close to be separately determined by least-squares fitting. The electron-capture cross sections are of the size of Coulomb-attractive positively charged traps, hence the donor designation. In addition, a low concentration ($\leqslant 10^{12}$ cm^{-2}) of acceptorlike electron traps was detected ($\sigma_{n3} \simeq 1\times 10^{-15}$ cm^2 in Table III) which anneals out at 800 °C in dry oxygen.

The oxide hole and electron traps have been found previously by other researchers. Aitken and Young[8] found a hole trap in "hardened" oxides, that is, oxides grown in such a way so as to minimize oxide charging by radiation. They found hole-capture cross sections 10^{-13} and 10^{-14} cm^2 and densities between 10^{12} and 10^{13} cm^{-2}. This agrees with the present results (σ_{p1} in Table III). Aitken and Young also found that postoxidation inert-gas (N_2 and Ar) anneals will increase the trap density. Powell[27] found hole-capture cross sections of 1.04×10^{-13} and 6.5×10^{-15} cm^2 in wet oxides. Only the smaller cross section was found in the dry oxides. The oxides grown for the present study were grown in resistance-heated fused-silicon reaction tubes, while Powell's oxides were grown in silicon furnace tubes. At oxidation temperatures, fused-silica tubes can permit enough water to permeate through the walls to significantly alter the oxidation rate.[2] It is possible that the oxides used in this study could be classified as "wet." Another difference in preparation is the inert-gas anneal used in this study. This anneal could have added the larger cross-section traps to the dry oxide, bringing the results of Powell and of this study into accord.

Ning[28] found positively charged electron traps in his MOS oxides. The cross section measured was 3×10^{-13} cm^2 at 7×10^5 V/cm. Electron-beam irradiation enhanced this trap. This value for the cross section is in excellent agreement with present data of σ_{n1} (Table III).

TABLE IV. Comparison of the total number of hole traps as determined by hole injection with that obtained from electron injection and trapping with $\sigma_{n1} = (3\text{–}6)\times 10^{-13}$ cm^2.

Device	$N_{TT1} + N_{TT2}$ (10^{12} cm^{-2})	$P_{T01} + \Sigma n_{Ti}$ (10^{12} cm^{-2})
10C-2	7.70 ± 0.06	7.3 ± 0.2
1061-3	6.44 ± 0.02	6.5 ± 0.3
106T-2	5.6 ± 0.1	5.5 ± 0.3
1081-1	4.96 ± 0.08	4.4 ± 0.08
1081-2	4.59 ± 0.04	4.3 ± 0.2
108T-1	4.1 ± 0.1	4.1 ± 0.1

TABLE V. Interface-state density near the silicon conduction band edge as determined by the low-temperature (77 K) C-V shift method. The anneal done here was 2 min at 400 °C in a forming gas (4% H_2, 96% N_2) ambient.

Device	Q_{IS}/q (10^{12} cm^{-2}) Before F. G. anneal	After F. G. anneal
10C-2	6.73	1.75
1061-3	1.63	1.23
106T-2	3.50	1.35
1081-2	5.37	1.20

V. DISCUSSION—OXIDE-DEFECT MODEL

In Sec. IV, evidence of two hole traps at the Si-SiO_2 interface was presented. The annealing behavior, where one trap density increases at the expense of another, suggests that one trap is being converted to the other during the post oxidation heat treatment in oxygen. Since the heat treatment is a low-temperature oxidation, the second trap is likely to be an oxidized species of the first.

The model proposed to explain the anneal behavior is that donor trap 1 (T_1) is trivalent silicon, $\equiv$Si·, and donor trap 2 (T_2) is nonbridging oxygen, $\equiv$Si $-$ O, The annealing can then be modeled by the reactions:

$$\equiv \text{Si}\cdot + \text{O} \underset{k_1'}{\overset{k_1}{\rightleftarrows}} \equiv \text{Si-O}, \tag{14}$$

$$T_1 + \text{O} \underset{k_2}{\rightleftarrows} T_2,$$

$$\equiv \text{Si}\cdot \equiv \text{Si-O} \rightarrow \text{Si-O-Si}, \tag{15}$$

$$T_1 + T_2 \rightarrow N_0,$$

where k_1, k_1', and k_2 are the reaction rates.

The first reaction is the oxidation of trivalent silicon and is assumed to be irreversible. The second reaction is needed to explain the simultaneous annealing of both traps at 800 °C (see Fig. 11). Note that reaction (15) is simply the annihilation of the traps. It is reasonable to assume that the distribution of the first and second traps are independent and random. The rate equations corresponding to these reactions are as follows:

TABLE VI. Results of fitting charge-trapping data to Eqs. (11) and (12). These data were taken after the forming gas anneal.

Device	N_{TT1} (10^{12} cm^{-2})	σ_{p1} (10^{-14} cm^2)	N_{TT2} (10^{12} cm^{-2})	σ_{p2} (10^{-15} cm^2)	Q (10^{12} cm^{-2})
Hole injection: $Q_{0X}+Q_{IS}=-N_{TT1}\exp(-\sigma_{p1}N^{+}_{INJ})-N_{TT2}\exp(-\sigma_{p2}N^{+}_{INJ})+Q$					
10C-2	7.62 ± 0.06	6.2 ± 0.1	...	...	7.75 ± 0.06
1061-3	6.31 ± 0.05	5.8 ± 0.1	...	...	7.66 ± 0.06
106T-2	2.7 ± 0.1	7.1 ± 0.4	2.40 ± 0.07	6.5 ± 0.7	6.24 ± 0.06
1081-2	1.53 ± 0.06	5.2 ± 0.3	1.24 ± 0.05	3.4 ± 0.4	3.66 ± 0.04

Device	p_{TO1} (10^{12} cm^{-2})	$\sigma_{n1}\leqslant\sigma_{n2}$ (10^{-13} cm^2)	Q (10^{12} cm^{-2})
Electron injection: $Q_{0X}+Q_{IS}=p_{TO1}\exp(-\sigma_{n1}N^{-}_{INJ})+Q$			
10C-2	7.2 ± 0.1	2.6 ± 0.1	0.12 ± 0.08
1061-3	5.48 ± 0.09	3.0 ± 0.1	1.2 ± 0.04
106T-2	5.02 ± 0.07	3.3 ± 0.1	1.04 ± 0.04
1081-2	2.45 ± 0.04	4.8 ± 0.2	1.04 ± 0.02

$$\frac{\partial N_{TT1}}{\partial t} = -k_1N_0N_{TT1}+k_1'N_{TT2}-k_2N_{TT1}N_{TT2}, \tag{16}$$

$$\frac{\partial N_{TT2}}{\partial t} = +k_1N_0N_{TT1}-k_1'N_{TT2}-k_2N_{TT1}N_{TT2}, \tag{17}$$

where N_0 is the density of bridging atomic oxygen. Note that N_{TT1} and N_{TT2} have dimensions in cm^{-2} while N_0 has dimensions in cm^{-3}.

N_0, the oxygen density near the interface, is essentially constant during the postoxidation heat treatment. This is because the oxidation of silicon is diffusion limited.[29,30] The rate of oxidation is determined by the diffusion of molecular oxygen through the oxide to the Si-SiO_2 interface. Using the value of the diffusivity of O_2 in SiO_2 found by Norton,[31] the diffusion lengths of oxygen in the thermal oxide layer during postoxidation heat treatment can be calculated. At 600 °C they are 4.4 and 13.8 μm for 1 and 10 h, respectively. At 800 °C the diffusion lengths are 18.4 and 38.2 μm for 1 and 10 h, respectively. Since the oxide thickness was 0.28 μm during the heat treatment, a steady-state oxygen flux was established early in the heat treatment. Also, since the oxide grew only 3.7 Å during 10 h at 800 °C according to the kinetic constants of Irene and van der Meulen,[32] the steady-state oxygen flux did not change. The oxygen flux must equal the reaction rate which in turn is proportional to N_0.[29] Therefore, N_0 is constant during the postoxidation heat treatment.

Equations (20) and (21) can be reduced to a convenient dimensionless form by defining the following variables and constants:

$$x = N_{TT1}/N^0_{TT1}, \tag{18a}$$

$$y = N_{TT2}/N^0_{TT1}, \tag{18b}$$

$$\tau = k_1N_0t, \tag{18c}$$

$$c_1 = k_1'k_1N_0, \tag{18d}$$

$$c_2 = k_2N^0_{TT1}/k_1N_0, \tag{18e}$$

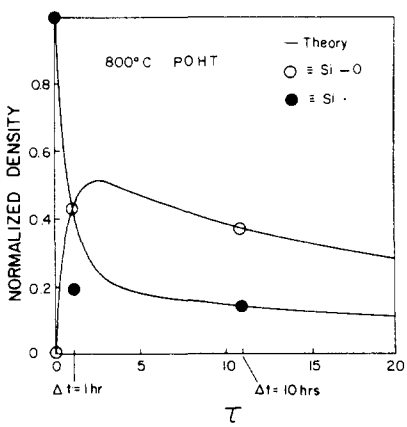

FIG. 12. Comparison of the nonbridging oxygen, ≡Si-O, and trivalent silicon, ≡Si·, densities at 800 °C with the annealing kinetics theory of Eqs. (14) and (15). The values of the parameters used are as follows: $K_1N_0=3.1\times10^{-4}$ sec^{-1}, $k_1'=6.2\times10^{-5}$ sec^{-1}, and $k_2=1.6\times10^{-17}$ cm^{-1} sec^{-1}. The normalization concentration is approximately 8×10^{12} cm^{-2}, as indicated in Fig. 11.

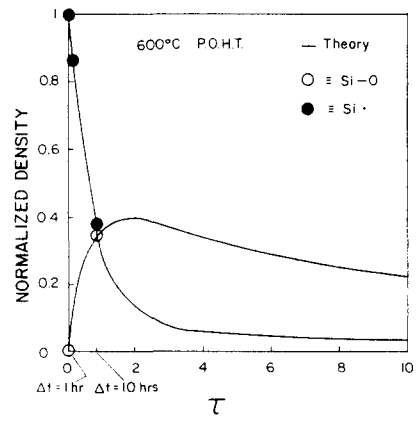

FIG. 13. Comparison of the nonbridging oxygen, ≡Si-O, and trivalent silicon, ≡Si·, densities at 600 °C with the annealing kinetics theory of Eqs. (14) and (15). The values of the parameters used are as follows: $k_1N_0=2.5\times10^{-5}$ sec^{-1}, $k_1'=2.5\times10^{-5}$ sec^{-1}, and $k_2=6.5\times10^{-19}$ cm^{-2} sec^{-1}. The normalization concentration is approximately 8×10^{12} cm^{-2}, as indicated in Fig. 11.

TABLE VII. Kinetic parameters of annealing reactions given by Eqs. (14) and (15).

Temperature (°C)	$k_1 N_0$ (sec^{-1})	k_1' (sec^{-1})	k_2 ($cm^{-2}\,sec^{-1}$)
600	2.5×10^{-5}	2.5×10^{-5}	6.5×10^{-19}
800	3.1×10^{-4}	6.2×10^{-5}	1.6×10^{-17}

where N_{TT1}^0 is the initial value of N_{TT1}. Equation (16) then becomes

$$\frac{\partial x}{\partial \tau} = -x + c_1 y - c_2 x y, \tag{19}$$

and Eq. (17) becomes

$$\frac{\partial y}{\partial \tau} = x - c_1 y - c_2 x y. \tag{20}$$

These simultaneous equations can be solved numerically. A fourth-order Runge-Kutta integration[33] was used. Since τ, c_1, and c_2 can vary with temperature, the 800 °C data of Table III (1081-1, 1081-2, and 108T-1) was fit separately by a trial-and-error method. The best fit to the data was found when $k_1 N_0 = 3.1\times10^{-2}\,sec^{-1}$, $c_1 = 0.2$, and $c_2 = 0.4$. The results of the analysis are shown in Fig. 12. The 600 °C data of Table III could be fit with the parameters $k_1 N_0 = 2.5\times10^{-5}\,sec^{-1}$, $c_1 = 1.0$, and $c_2 = 0.2$. The results of this analysis are shown in Fig. 13. The value for N_{TT1} after a 1-h heat treatment at 800 °C is overestimated by the theory. Apparently, there is another mechanism present to reduce the density of the first trap. In light of the small amount of data at this stage of the analysis, a more complex model of the annealing reactions cannot be proposed.

At this point we wish to test the identification of the first trap ($\sigma_{p1} = 6\times10^{-14}\,cm^2$) with trivalent silicon, ≡Si·, and the second trap ($\sigma_{p2} = 10^{-15}\,cm^2$) with nonbridging oxygen, ≡Si-O. These defects satisfy the reactions given in Eqs. (14) and (15) and are intrinsic network defects of SiO_2. These reactions require that two of the first traps initially be near each other for both reactions to take place. A full oxygen vacancy, which is known to exist in SiO_2, is two trivalent silicon centers near each other.[22] Thus, with the above identification, the sequence of the two traps is plausible.

The values for the kinetic parameters, k_1, N_0, k_1', and k_2, are listed in Table VII. For k_2 to be accurately determined and for the model to be quantitatively tested, more data is needed at long annealing times, where the second annealing reaction [Eq. (15)] can be made dominant. The rate of dissociation of the oxidized defect, T_2, is k_1'. The activation energy of k_1' was found to be 0.4 eV from the data of Table VII. This does not agree with the Si-O band energy of 3.82 eV[34] and suggests that impurities instead of oxygen might be responsible for the annealing behavior.

VI. CONCLUSIONS

The VUV-bias method is a useful tool in the characterization of MOS oxides. This low-field electron- or hole-injection method charges oxide traps so that they can be detected by a standard capacitance-voltage measurement. The kinetics of charging can be analyzed to characterize the oxide traps in terms of their capture cross sections. The capacitance-voltage measurements can be automated for fast and consistent data acquisition and analysis.

Two hole traps were found in our thermally grown SiO_2 in dry oxygen with hole capture cross sections of 6×10^{-14} and $1\times10^{-15}\,cm^2$. The maximum densities of these traps were 7.7×10^{12} and $3.4\times10^{12}\,cm^{-2}$, respectively. These traps appear to be donorlike, i.e., neutral before capturing a hole. These same traps, positively charged after hole capture, become efficient electron traps with a nearly equal electron-capture cross section of $3\times10^{-13}\,cm^2$. In addition, an acceptorlike electron trap with an electron-capture cross section of $10^{-15}\,cm^2$ was also detected which anneals out at 800 °C in dry oxygen.

Photocurrent-vs-voltage measurements locate the charge within 50 Å of the Si-SiO_2 interface. A smaller amount of negative charge was sometimes found at the aluminum-silicon dioxide interface.

As the oxide traps are charged positively by VUV hole injection there is no change in the interface-state charge density. The oxide charge studied here neither generates interface states by breaking bonds not induces interface states by adding a perturbation to the interface potential. The oxide traps detected in this study must be 5 Å or more from the Si-SiO_2 interface, otherwise, the trapped charges can tunnel to the silicon instead of giving the time-independent density after the charging or discharging experiment.

These traps are generated during the oxidation and inert-gas anneal steps, both of which are done at high temperatures: 1000 or 1100 °C. More traps are found when the oxide was grown at 1100 °C than at 1000 °C.

The traps can be annealed out at 600 and 800 °C. Their annealing behavior was modeled to determine the nature of the oxide traps. The annealing reactions were compared to the oxidation of trivalent silicon, converting it into nonbridgin oxygen, and the healing of a Si-O-Si bond by the recombination of adjacent trivalent silicon and nonbridging oxygen. Qualitative agreement was found.

ACKNOWLEDGMENTS

This work was based on a doctoral thesis of A. R. S. and supported by the Air Force Office of Scientific Research (grant AFOSR 78-3714) and Rome Air Development Center (contract RADC-F-19628-C-0138). A. R. S. was also supported by a University of Illinois Graduate Fellowship and is currently with Intel Corporation, Santa Clara, where some revision of the manuscript was made.

[1] C. R. Helms, N. M. Johnson, S. A. Schwarz, and W. E. Spicer, *Proceedings of the International Conference at Yorktown Heights, N.Y., 1978* (Pergamon, New York, 1978), p. 366; Pergamon Press, J. Appl. Phys. **50**, 7007 (1979).
[2] A. G. Revesz, J. Non-Cryst. Solids **11**, 309 (1973).
[3] K. G. Aubuchon, IEEE Trans. Nucl. Sci. **NS-18**, 117 (1971).
[4] G. F. Derbenwick and B. L. Gregory, IEEE Trans. Nucl. Sci. **NS-18**, 2151 (1975).

[5]E. H. Snow, A. S. Grove, and D. J. Fitzgerald, Proc. IEEE **55**, 1168 (1967).
[6]E. P. Eer Nisse and G. F. Derbenwick, IEEE Trans Nucl. Sci. **NS-23**, 1534 (1976).
[7]C. N. Berglund and R. J. Powell, J. Appl. Phys. **42**, 573 (1971).
[8]J. M. Aitken and D. R. Young, IEEE Trans. Nucl. Sci. **NS-24**, 2128 (1977).
[9]T. H. Ning, P. W. Cook, R. H. Dennard, C. M. Osburn, S. E. Schuster, and H-N Yu, IEEE Trans. Electron. Dev. **ED-26**, 346 (1979).
[10]R. J. Powell and G. F. Derbenwick, IEEE Trans. Nucl. Sci. **NS-18**, 99 (1971).
[11]A. G. Holmes-Seidle and I. Groombridge, Thin Solid Films **27**, 165 (1975).
[12]K. H. Zaininger and A. G. Holmes-Seidle, RCA Rev. **28**, 208 (1967).
[13]C. T. Sah, T. H. Ning, and L. L. Tschopp. Surf. Sci. **32**, 561 (1972).
[14]D. J. DiMaria, Z. A. Weinberg, and J. M. Aitken, J. Appl. Phys. **48**, 898 (1977).
[15]Z. A. Weinberg, G. W. Rubloff, and E. Bassous, Phys. Rev. B **19**, 3107 (1979).
[16]L. M. Terman, Solid-State Electron. **5**, 285 (1962).
[17]M. J. McNutt and C. T. Sah, J. Appl. Phys. **46**, 3909 (1975).
[18]C. T. Sah, R. F. Pierret, and A. B. Tole, Solid-State Electron. **12**, 681 (1969).
[19]M. J. McNutt and C. T. Sah, Solid State Electron. **17**, 377 (1974).
[20]D. J. DiMaria, J. Appl. Phys. **47**, 4073 (1976).
[21]R. J. Powell and C. N. Berglund, J. Appl. Phys. **42**, 4390 (1971); R. J. Powell, IEEE Trans. Nucl. Sci. **NS-22**, 2240 (1975).
[22]C. T. Sah, IEEE Trans. Nucl. Sci. **NS-23**, 1563 (1976).
[23]M. H. Cohen, J. Non-Cryst. Solids **4**, 391 (1970).
[24]E. H. Nicollian and A. Goetzberger, Bell. Syst. Tech. J. **46**, 1055 (1967); D. E. Eaton, Solid-State Electron. **16**, 841 (1973).
[25]C. S. Shiue and C. T. Sah, Phys. Rev. B **19**, 2149 (1979); Surf. Sci. **98**, 173 (1980).
[26]M. Lax, Phys. Rev. **119**, 1502 (1960).
[27]R. J. Powell (unpublished).
[28]T. H. Ning, J. Appl. Phys. **49**, 4077 (1978).
[29]J. Blanc, Appl. Phys. Lett. **33**, 424 (1978).
[30]B. E. Deal and A. S. Grove, J. Appl. Phys. **36**, 3770 (1965).
[31]F. J. Norton, Nature **191**, 701 (1961).
[32]E. A. Irene and Y. J. Van der Meulen, J. Electrochem. Soc. **123**, 1380 (1976).
[33]*Handbook of Mathematical Functions*, edited by M. Abramowitz and I. A. Stegun (Dover, New York, 1964), Item 25.5.18, p. 897.
[34]L. Pauling, *The Nature of the Chemical Bond*, 3rd ed. (Cornell University Press, Ithaca, N. Y., 1960), p. 85.